Gas1 extends the range of Hedgehog action by facilitating its signaling

David C. Martinelli[1,2] and Chen-Ming Fan[1,3]

[1]Department of Embryology, Carnegie Institution of Washington, Baltimore, Maryland 21218, USA; [2]Department of Biology, Johns Hopkins University, Baltimore, Maryland 21218, USA

Cellular signaling initiated by Hedgehog binding to Patched1 has profound importance in mammalian embryogenesis, genetic disease, and cancer. Hedgehog acts as a morphogen to specify distinctive cell fates using different concentration thresholds, but our knowledge of how the concentration gradient is interpreted into the activity gradient is incomplete. The membrane protein Growth Arrest-Specific Gene 1 (GAS1) was thought to be a negative regulator of the Hedgehog concentration gradient. Here, we report unexpected genetic evidence that *Gas1* positively regulates Hedgehog signaling in multiple developmental contexts, an effect particularly noticeable at regions where Hedgehog acts at low concentration. Using a combination of in vitro cell culture and in ovo electroporation assays, we demonstrate that GAS1 acts cooperatively with Patched1 for Hedgehog binding and enhances signaling activity in a cell-autonomous manner. Our data support a model in which GAS1 helps transform the Hedgehog protein gradient into the observed activity gradient. We propose that *Gas1* is an evolutionarily novel, vertebrate-specific Hedgehog pathway regulator.

The Hedgehog pathway features a cholesterol and palmitate modified, 19-kDa secreted Hedgehog protein (Porter et al. 1996; Pepinsky et al. 1998). In mammals, *Indian Hedgehog* (*Ihh*) and *Sonic Hedgehog* (*Shh*) encode two proteins responsible for all early embryonic Hedgehog function. "HH" will be used here to refer to properties common to both. They elicit pathway activation primarily through binding to the Patched1 (PTC1) protein, which, in turn, allows the Smoothened (SMO) protein to initiate a cascade of events leading to activity modulation of the GLI transcription factor family and regulation of downstream genes (Briscoe and Ericson 1999). Although the majority of HH protein is believed to be membrane bound, limiting it to local signaling, a small fraction can become soluble and diffuse to long distances (Zeng et al. 2001). The concentration gradient of the diffusible HH is transformed into graded signaling strengths in responding cells to specify them to an array of cell fates. To achieve a defined pattern of cell types within the target field, the contour of the gradient is finely tuned by HH-binding proteins such as PTC1. *Ptc1* is directly up-regulated by HH, thus providing a negative feedback loop to limit the range of diffusion by presenting additional binding sites for HH (Chen and Struhl

1996). The feedback loop predicts a sequestration of HH near its source, creating a steep gradient (Saha and Schaffer 2006). This causes a potential problem at the fringe of the patterning field, where HH protein may not be concentrated enough for pathway activation and requires signal enhancing mechanisms. Understanding the mechanisms through which HH signaling strength is regulated is of great importance for understanding not only embryogenesis but also genetic diseases and cancers caused by misregulated HH signaling (McMahon et al. 2003; Xie 2005; Kayed et al. 2006).

Gas1 (*Growth Arrest-Specific Gene 1*) encodes a 37-kDa, N-glycosylated, and glycosylphosphatidyl inositol (GPI)-linked plasma membrane protein. It was first discovered as a negative cell cycle regulator and tumor suppressor in cultured cells (Schneider et al. 1988; Del Sal et al. 1994; Evdokiou and Cowled 1998). We found that GAS1 has a high affinity for HH and suggested that it has a potential role in regulating HH signaling (Lee et al. 2001a). However, the role for *Gas1* in HH signaling during normal development has not been established. Here we present a direct measure of the genetic interaction between *Gas1* and *Shh* to demonstrate that *Gas1* is an enhancer of HH signaling, particularly at a long distance and/or at low concentrations. Combined with the finding that HH signaling negatively regulates *Gas1* expression, we propose a model in which GAS1 fine-tunes the HH activity gradient.

[3]Corresponding author.
E-MAIL fan@ciwemb.edu; FAX (410) 243-6311.
Article is online at http://www.genesdev.org/cgi/doi/10.1101/gad.1546307.

Results

Generation of the Gas1[LacZ] *allele*

To facilitate visualization and study the regulation of *Gas1* expression, we generated a mouse line in which the *Gas1* coding region is replaced by a *LacZ* gene. The LacZ reporter activity reproduces the expression pattern of *Gas1* as previously obtained by in situ hybridization (ISH) (Supplementary Fig. S1; Lee and Fan 2001). Mice heterozygous for this mutant allele are phenotypically normal, and homozygous mutant embryos have the same phenotypes as the original *Gas1* mutant; for example, defects in the limb and eye (Lee et al. 2001b; Liu et al. 2002). This *LacZ* allele was used for all genetic crosses in this study and is referred to as *Gas1⁻* for simplicity.

Gas1 *and* Shh *interact genetically*

Overexpression of *Gas1* in tissue explants demonstrated that it could function as an antagonist to HH signaling in vitro (Lee et al. 2001a; Cobourne et al. 2004). To test this in vivo, we sought to define the relationship between *Gas1* and *Shh* by genetic analysis. We generated mice that were double heterozygous for *Gas1⁻* and a mutant

allele of *Shh* ($Gas1^{+/-};Shh^{+/-}$) (Chiang et al. 1996), which were phenotypically normal. These mice were interbred to obtain embryos of allelic combinations for analysis. Morphological analysis of neonatal mice revealed that $Gas1^{-/-};Shh^{+/-}$ mice have a single nostril as opposed to the normal two found in $Gas1^{+/-};Shh^{+/-}$ and $Gas1^{-/-}$ mice (Fig. 1A–C). Narrowing and fusion of midline facial structures represents a mild holoprosencephaly, a birth defect associated with impaired SHH signaling (Roessler and Muenke 2003). Curiously, $Gas1^{-/-};Shh^{-/-}$ pups were not found at birth, suggesting embryonic lethality. We found that the double mutants were only recovered at a ratio (0.053) close to the Mendelian ratio (0.0625) at 9.5 d of embryonic development (E9.5) (Fig. 1D), unlike $Shh^{-/-}$ or $Gas1^{-/-}$ embryos, which can survive to term. $Gas1^{-/-};Shh^{-/-}$ embryos were less frequently recovered at E10.5, but were morphologically arrested at E9.5, indicating lethality around E9.5.

Gross morphological examination of E9.5 embryos revealed that the *Gas1;Shh* double mutants were more severely affected than either single mutant. The double mutants had a reduced size and inflated pericardium, and failed to undergo proper embryonic turning, resulting in a double-kink in the body axis or an L-shaped body axis (Fig. 1E–H). They also had severe cardiac edema, presum-
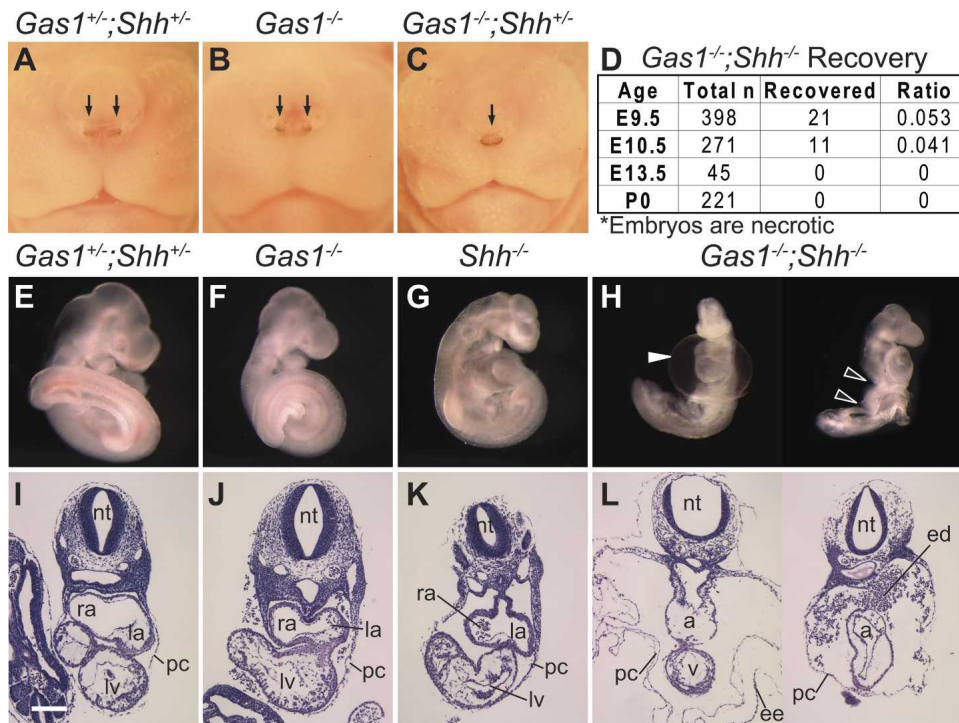

Figure 1. A genetic interaction exists between *Gas1* and *Shh*. Neonatal control (*A*) and $Gas1^{-/-}$ (*B*) mice have two nostrils (arrows), while $Gas1^{-/-};Shh^{+/-}$ (*C*) mice have one (*n* = 5). (*D*) The table shows the recovery of $Gas1^{-/-};Shh^{-/-}$ embryos at different stages from crosses between $Gas1^{+/-};Shh^{+/-}$ mice. (*E–H*) Gross morphology comparison between day 9.5 embryos of different genotypes (as labeled): The $Gas1^{-/-};Shh^{-/-}$ embryos have an inflated pericardium (arrowhead, ventral view) and a double-kinked body axis (open arrowheads, lateral view with pericardium removed). (*I–L*) Hematoxylin and eosin staining of transverse sections at similar levels of the heart at E9.5: For the $Gas1^{-/-};Shh^{-/-}$ embryos, note the failed heart tube looping compared with the other genotypes; in the *right* panel of *L*, the ventricle is not present at this level of section. (a) Atrium; (ed) edema; (ee) extra embryonic membrane; (la) left atrium; (lv) left ventricle; (nt) neural tube; (pc) pericardium; (ra) right atrium; (v) ventricle. Bar: *I –L*, 200 μm.

ably the cause of lethality. Histological analysis of transverse sections at the level of the heart reveals a linear or mostly linear heart tube in the $Gas1^{-/-};Shh^{-/-}$ embryos (Fig. 1I–L), indicating a defect in left/right heart asymmetry, a process dependent on combined SHH and IHH signaling in the node (Zhang et al. 2001).

The morphological defects described above for $Gas1^{-/-};Shh^{-/-}$ embryos are similar to but not as severe as those described for $Smo^{-/-}$ and $Shh^{-/-};Ihh^{-/-}$ embryos, both of which have a complete loss of early embryonic HH signaling (Zhang et al. 2001). These correlations and genetic interactions described above lead us to propose that *Gas1* acts positively in HH signaling, instead of the previously proposed antagonistic relationship obtained in vitro (Lee et al. 2001a; Cobourne et al. 2004).

Gas1 *facilitates HH signaling in the neural tube and somite*

To define *Gas1*'s genetic contribution to HH signaling at the molecular level, we examined the somites and neural tube of $Gas1^{-/-}$ and $Gas1^{-/-};Shh^{-/-}$ embryos. The somites are the embryonic precursors that form the vertebrae and ribs, while the neural tube forms the spinal cord at the trunk level. HH signaling regulates the pattern of gene expression along the dorso–ventral axis of both systems. SHH is the primary source, secreted first from the notochord located just ventral to the neural tube, and then from the floorplate after it is induced by the notochord (Fig. 2U; Litingtung and Chiang 2000a). Localized HH positively regulates downstream gene expression in the ventral portions of the somites and neural tube, and negatively regulates genes to restrict their expression to the dorsal somite and neural tube. If *Gas1* acts positively in HH signaling, then when *Gas1* function is removed, we expect to observe reductions in ventral marker expression and expansions in dorsal marker expression.

To monitor the dorso–ventral polarity of the somite at the forelimb level of E9.5 embryos, we used *Pax1*, a ventral marker activated by HH, as well as *Pax3* and PAX7, dorsal markers repressed by HH (Fan and Tessier-Lavigne 1994). In the $Gas1^{-/-}$ somite, the *Pax1* domain appeared not to extend as far dorsally compared with the $Gas1^{+/-};Shh^{+/-}$ control (Fig. 2A,B), while the domains of *Pax3* and PAX7 appeared normal (Fig. 2E,F,I,J). In the $Shh^{-/-}$ embryo, residual HH signaling to the somite is still present due to partial compensation by IHH secreted from the endoderm located ventral to the notochord (Zhang et al. 2001). As published, we found that there was *Pax1* expression in the $Shh^{-/-}$ somite, but at a reduced level and more ventrally restricted (Fig. 2C), while *Pax3* and PAX7 expression was ventrally expanded (Fig. 2G,K; Chiang et al. 1996). In the $Gas1^{-/-};Shh^{-/-}$ embryo, *Pax1* expression was absent, suggesting a loss of HH pathway activation in the somites (Fig. 2D). Consistent with this, *Pax3* and PAX7 expression in the double mutant expands farther ventrally than in the *Shh* mutant (Fig. 2H,L). These results suggest that *Gas1* acts positively in HH signaling to the somites, and that its genetic contribution is particularly significant when the somite is only exposed to low-level HH signaling as in the *Shh* mutant.

HH primarily secreted from the notochord specifies multiple cell types in the ventral neural tube in a concentration-dependent manner (Ericson et al. 1995a,b; Tanabe et al. 1995; Briscoe et al. 1999). Among these cell types, the floorplate requires the highest HH concentration (via a contact-dependent process), while the p0 progenitors require the lowest (Briscoe et al. 2001; Pierani et al. 2001). Based on the above findings, we examined markers known to be indicative of low-level HH signaling: *Dbx1*, which is expressed specifically in the p0 progenitors, and *Pax3* and PAX7, which are restricted to the dorsal neural tube due to repression by HH (Ericson et al. 1996). Importantly, the expression domains of these genes are encompassed by the *Gas1* expression domain (data not shown). In the E9.5 $Gas1^{-/-}$ embryo at the forelimb level, the *Dbx1* expression domain was ventrally expanded (Fig. 2M,N; Supplementary Fig. S2). The ventral boundaries of *Pax3* and PAX7 expression shifted slightly ventrally as well (Fig. 2E,F,I,J; Supplementary Fig. S2). Quantitation of marker expression boundaries and additional marker analysis were performed to document the neural tube defect of $Gas1^{-/-}$ and $Gas1^{-/-};Shh^{+/-}$ embryos in Supplementary Figure S2. These data collectively indicate that in the $Gas1^{-/-}$ background, there is reduced HH signaling.

As previously described, *Dbx1* expression in the $Shh^{-/-}$ neural tube was shifted ventrally to the midline (Fig. 2O) accompanied by the ventral expansion of *Pax3* and PAX7 expression (Fig. 2G,K; Litingtung and Chiang 2000b; Wijgerde et al. 2002). This *Dbx1*-positive domain is most likely mediated by diffusible IHH from the endoderm (Zhang et al. 2001; Wijgerde et al. 2002). In the $Gas1^{-/-};Shh^{-/-}$ neural tube, there was a complete lack of *Dbx1* expression (Fig. 2P), and *Pax3* and PAX7 expression expanded farther ventrally to encompass the entire neural tube (Fig. 2H,L). Thus, although the defect of the $Gas1^{-/-}$ neural tube is subtle, *Gas1*'s contribution to IHH signaling becomes clear in the sensitized $Shh^{-/-}$ background. This conclusion is further confirmed by the expression of the HH target *Ptc1* (Goodrich et al. 1996; Marigo and Tabin 1996), which becomes progressively more ventrally restricted from the $Gas1^{+/-};Shh^{+/-}$, to the $Gas1^{-/-}$, the $Shh^{-/-}$, and finally the $Gas1^{-/-};Shh^{-/-}$ genotype (Fig. 2Q–T). There remains residual *Ptc1* expression in the $Gas1^{-/-};Shh^{-/-}$ neural tube, likely due to its basal transcription level.

While the above results suggest that *Gas1* facilitates HH signaling, it is also possible that *Gas1* regulates HH expression. To test this, we examined the expression of IHH and *Shh*. We found that IHH production in the endoderm is similar between the $Gas1^{-/-};Shh^{-/-}$ embryo and the $Shh^{-/-}$ embryo (Fig. 2W,X), supporting that in the $Shh^{-/-}$ embryo, *Gas1* facilitates IHH signaling to the neural tube and somites. In $Gas1^{-/-}$ embryos, we found normal levels of *Shh* expression in the notochord. Interestingly, we found a narrow, triangular-shaped floorplate instead of the normal wedge shape, reflected by a
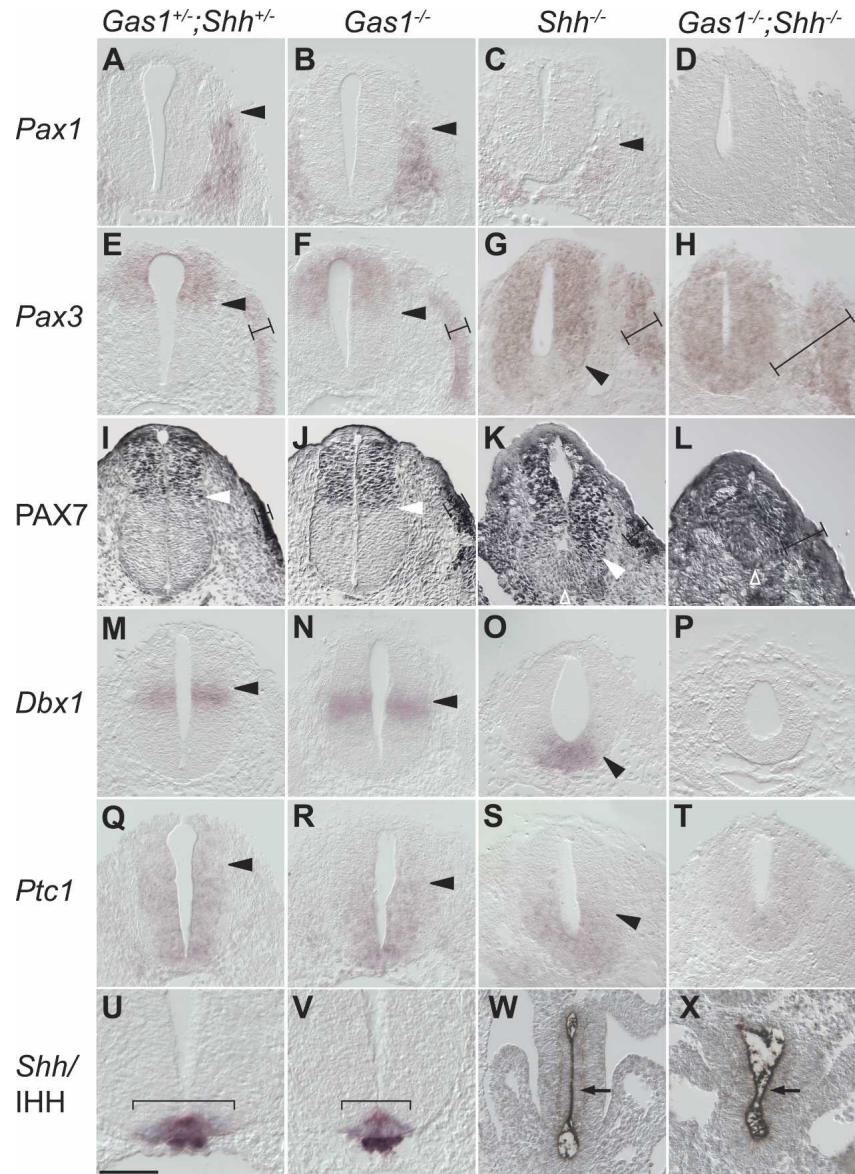
Figure 2. Compensation provided by IHH signaling in the $Shh^{-/-}$ background is eliminated in $Gas1^{-/-};Shh^{-/-}$ embryos. (*A–D*) *Pax1* ISH (*n* = 11). (*E–H*) *Pax3* ISH (*n* = 15). (*I–L*) PAX7 IHC (*n* = 9). (*M–P*) *Dbx1* ISH (*n* = 5). (*Q–T*) *Ptc1* ISH (*n* = 11). Arrowheads indicate the dorsal or ventral extent of gene expression; lines in *E–H* indicate the domain size of *Pax3* and PAX7. (*U,V*) *Shh* ISH (*n* = 3); brackets indicate the width of *Shh*-expressing floorplate cells; images are at 2× higher magnification. (*W,X*) IHH IHC (*n* = 2); arrows indicate the apical localization of IHH protein. All sections are transverse at the forelimb level of E9.5 embryos. Genotypes are labeled on *top* of each panel. Not shown are $Gas1^{+/-};Shh^{-/-}$ embryos, which display a variable but intermediate phenotype between $Shh^{-/-}$ and $Gas1^{-/-};Shh^{-/-}$. Axis: Dorsal is up, ventral is down. Bars: all except for *U,V*, 100 µm; *U,V*, 50 µm.

reduced *Shh* expression domain (Fig. 2U,V). This suggests that *Gas1* aids SHH signaling from the notochord to induce the floorplate. *Gas1* is expressed throughout the entire neural tube at earlier stages of development during floorplate induction (data not shown; see below), consistent with a role for *Gas1* in floorplate induction. However, the relative contribution to the $Gas1^{-/-}$ neural tube phenotype at E9.5 caused by the lack of *Gas1* versus a secondary consequence of the reduced size of the *Shh*-positive floorplate is not clear.

Gas1 *facilitates low-level SHH signaling in the limb*

The above-described phenotypes suggest that either *Gas1* generally facilitates HH signaling or that *Gas1* acts preferentially with IHH. To test whether *Gas1* also facilitates SHH, we examined the developing limbs, an established system for studying SHH signaling without input from other HH homologs. A current model for the role of SHH in patterning digit number and identity along the anterio–posterior (A/P) axis states that digit 1 is SHH-independent; digit 2 and the anterior part of digit 3 receive only diffusible SHH; and digits 4 and 5 and the posterior part of 3 are specified at least in part by the different lengths of time exposed to local SHH signaling (Chiang et al. 2001; Kraus et al. 2001; Ahn and Joyner 2004; Harfe et al. 2004). If *Gas1* also facilitates SHH signaling, we would expect impaired digit specification by removing *Gas1* function.

To test this, skeletal preparations of neonatal $Gas1^{+/-};Shh^{+/-}$, $Gas1^{-/-}$, and $Gas1^{-/-};Shh^{+/-}$ limbs were performed. Digit numbers on limbs were scored as having either a normal five digits, four, or 4.5 (five digits with digit 2 being fused to either digit 1 or 3). When

compared with $Gas1^{+/-};Shh^{+/-}$ controls, $Gas1^{-/-}$ limbs had an overall reduced size, a disproportionately smaller digit 2 (Supplementary Fig. S3), and hypodactyly at a low penetrance (5% of forelimbs and 41% hindlimbs had 4.5 digits; 42% of hindlimbs were missing digit 2) (Fig. 3, cf. A,D and B,E), similar to the previously reported *Gas1* mutant (Liu et al. 2002). While the size of the limb remained constant, the digit 2 hypodactyly phenotype became exacerbated when *Shh* dosage was reduced in the $Gas1^{-/-};Shh^{+/-}$ background (16% of forelimbs had 4.5 digits; 84% of forelimbs and 100% of hindlimbs were missing digit 2) (Fig. 3C,F). Our rationale for suggesting that 2 is the identity of the missing digit is based on the morphology of the remaining digits and time-course

Figure 3. $Gas1^{-/-};Shh^{+/-}$ limbs have reduced range of SHH signaling. (*A–F*) Alcian blue-stained (for cartilage) and alizarin red-stained (for bone) neonatal forelimb (F.L.) and hindlimb (H.L.) autopods of $Gas1^{+/-};Shh^{+/-}$ (*A,D*) (n = 22), $Gas1^{-/-}$ (*B,E*) (n = 22), and $Gas1^{-/-};Shh^{+/-}$ (*C,F*) (n = 19) genotypes. (*G–R*) Whole-mount ISH of E10.5 forelimb buds: (*G–I*) *Fgf4* (n = 6). (*J–L*) *Grem* (n = 3). (*M–O*) *Ptc1* (n = 7); *Gli1* (not shown; n = 5); arrowheads mark the anterior boundary of expression. (*P–R*) *Shh* (n = 5). Axis: Anterior is up, posterior is down. Bars: *A–F*, 1 mm; *G–R*, 100 μm.

analysis revealing that a digit at the digit 2 position never forms in the $Gas1^{-/-};Shh^{+/-}$ genotype (Supplementary Fig. S3 and legend). The $Gas1^{-/-};Shh^{+/-}$ limbs closely resemble those hypomorphic for *Dispatched* (in a $Disp^{hypomorph/-};Shh^{+/-}$ background), which are defective in long-range SHH signaling and specifically lack digit 2 (Harfe et al. 2004). Together, these results support the model that *Gas1* facilitates long-range SHH signaling in the limb.

If this hypothesis is correct, then we expect to find a reduction in the expression of SHH downstream genes in the E10.5 limb bud, an early time period when SHH acts upon the limb. *Shh* is expressed in a posterior region of mesenchyme known as the Zone of Polarizing Activity (ZPA) (Fig. 3P). From E9.25, a stage prior to *Shh* expression in the ZPA, to E11.5, *Gas1* is not expressed in the posterior mesenchyme (see below; Liu et al. 2002). *Ptc1* and *Gli1* are SHH target genes, while *Fgf4* and *Grem* are indirectly activated, but their expression is also indicative of the range of SHH signaling. All are expressed in the mesenchyme, except for *Fgf4*, which is expressed in the Apical Ectodermal Ridge. Whole-mount ISH for these target genes reveals a more posteriorly restricted expression domain in the $Gas1^{-/-}$ limb bud when compared with the $Gas1^{+/-};Shh^{+/-}$ limb bud (Fig. 3, cf. G,J,M and H,K,N; data not shown). A further restriction is seen in the $Gas1^{-/-};Shh^{+/-}$ limb bud (Fig. 3I,L,O; data not shown). Importantly, target gene expression in the posterior regions close to or in the ZPA was unaffected, regions where *Gas1* is not expressed. *Shh* expression is not reduced in the $Gas1^{-/-};Shh^{+/-}$ limb when compared with that in the $Gas1^{+/-};Shh^{+/-}$ limb, indicating that the results of the marker analysis are not caused by *Shh* down-regulation (Fig. 3P,R). Therefore, our molecular analysis supports that *Gas1* is required for the full range of SHH signaling in the limb. More specifically, *Gas1* facilitates SHH signaling where it is expressed, which in the case of the limb bud corresponds to regions reached by only long-range and thus low-level SHH signaling.

SHH signaling inhibits the processing of the GLI3 (190 kDa) transcription factor into smaller forms (83 and 75 kDa), which function as strong transcriptional repressors (GLI3-R) (Wang et al. 2000). For patterning of digit number and identity, it is thought that the primary action of the SHH gradient in the limb bud is to establish a countergradient of the ratio of the GLI3-R to unprocessed GLI3 (GLI3-R:GLI3-190) (Litingtung et al. 2002). In the absence of *Gli3*, limbs form an array of seven to nine digits, each without a clear identity; this is observed regardless of the presence of *Shh*—that is, *Gli3* is epistatic to *Shh* (Litingtung et al. 2002). Based on the above results that *Gas1* facilitates HH signaling in the limb, we predict *Gli3* to also be epistatic to *Gas1* in digit patterning. To test this, we analyzed $Gli3^{-/-}$ and $Gas1^{-/-};Gli3^{-/-}$ limb digit patterns by skeletal preparation and observed that the polydactyly phenotype of $Gli3^{-/-}$ limbs is indistinguishable from that of $Gas1^{-/-};Gli3^{-/-}$ limbs, consistent with our hypothesis (Fig. 4A). Additionally, we predict to observe increases in the processing of GLI3-190 in
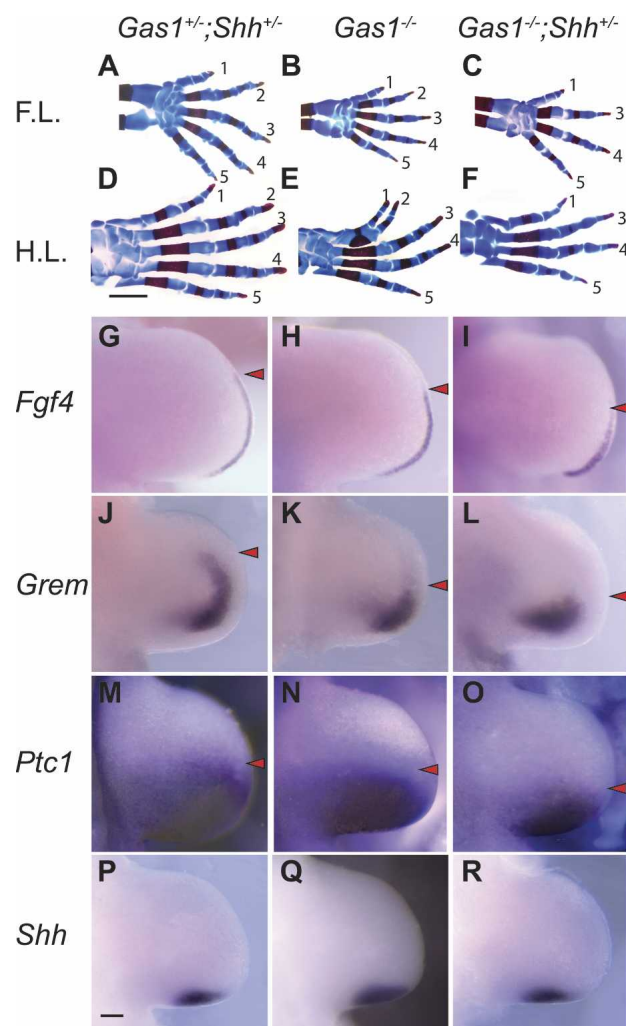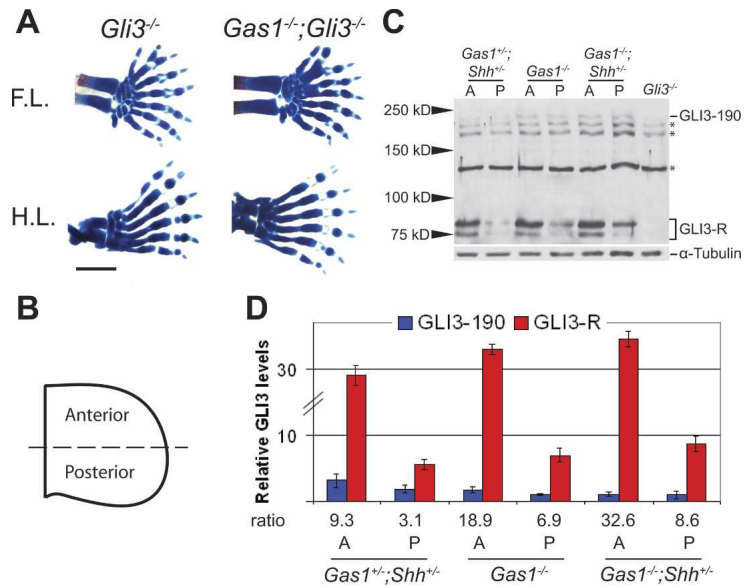
Figure 4. *Gli3* is epistatic to *Gas1* in digit patterning, and *Gas1* inhibits GLI3 processing. (*A*) Alcian blue- and alizarin red-stained E16.5 forelimb (F.L.) and hindlimb (H.L.) autopods of *Gli3⁻/⁻* and *Gas1⁻/⁻;Gli3⁻/⁻* limbs (*n* = 5). Bar, 1 mm. (*B*) Diagram depicting how E10.5 limb buds were dissected. (*C*) Western blot analysis for GLI3 on indicated genotype and limb bud halves. (A) Anterior; (P) posterior. GLI3-190 and GLI3-R bands are as labeled. A *Gli3⁻/⁻* limb bud was used for a control. Blots were stripped and reprobed for α-tubulin for a loading control. Asterisks indicate nonspecific bands. (*D*) Western blot repeated for three embryos of each genotype and band intensity quantified. GLI3-R:GLI3-190 ratios are indicated.

E10.5 limb buds that correlate with the phenotypes of the *Gas1⁻/⁻* and *Gas1⁻/⁻;Shh⁺/⁻* limbs. To test this, we harvested E10.5 limb buds, dissected each into anterior and posterior halves (Fig. 4B), and performed Western blot analysis using an antibody that recognizes all GLI3 forms (Fig. 4C). The intensity of the GLI3-190 and GLI3-R bands was quantified and normalized to α-tubulin, and the GLI3-R:GLI3-190 ratio was calculated (Fig. 4D). Similar to previously reported results, we found that the ratio was 9.3 in the anterior of control limb buds and 3.1 in the posterior (Wang et al. 2000). Importantly, in the *Gas1⁻/⁻* and *Gas1⁻/⁻;Shh⁺/⁻* buds, these ratios were increased by approximately twofold and threefold, respectively. How the measured changes of GLI3 isoform ratios in the mutant limbs are translated into the final digit patterns remains unresolved. However, the genetic and biochemical analyses above demonstrate that the relationship between *Gas1* and *Gli3* is consistent with *Gas1* facilitating HH signaling.

Gas1 *enhances the activity of SHH*

Taken together, our genetic analysis strongly supports a model in which *Gas1* is required for the complete range of HH signaling. We next investigated two possible mechanisms for how GAS1 could facilitate HH signaling, which are not necessarily mutually exclusive. First, GAS1 could enhance the diffusion or transport of HH protein to cells distant from the source of HH synthesis. Second, after HH has arrived at a target cell, GAS1 could enhance the ability of HH to induce signal transduction; that is, HH activity. To differentiate between these two possibilities, we first examined the distribution of SHH in E10.5 limb buds in the various allelic combinations of *Gas1* and *Shh* using immunohistochemistry (IHC), an established method used to determine the range of SHH diffusion (Gritli-Linde et al. 2001; Lewis et al. 2001;

Harfe et al. 2004). We found no detectable difference in the domain of SHH between the *Gas1⁺/⁻;Shh⁺/⁻* and *Gas1⁻/⁻;Shh⁺/⁻* genotypes (Fig. 5A) in contrast to the reduced SHH domain observed in the *Disp^(hypomorph/−);Shh⁺/⁻* limb bud (Harfe et al. 2004). Western blot analyses of E10.5 limb buds also showed that total SHH protein is not reduced in the *Gas1⁻/⁻;Shh⁺/⁻* limb bud when compared with *Gas1⁺/⁻;Shh⁺/⁻*, indicating that SHH production and stability are not altered (data not shown). However, since IHC may not be sensitive enough to detect the entire range of SHH distribution, it is possible that a subtle change in SHH diffusion might escape our detection.

The lack of evidence for a change of SHH diffusion in the *Gas1* mutant limbs led us to test whether GAS1 enhances SHH signaling activity. We chose to use an in vitro system uncomplicated by dependence on SHH diffusion. NIH3T3 cells with a stably integrated HH-responsive luciferase reporter gene driven by GLI-binding sites (NIH3T3-GLI-Luc) were transfected with either control or targeted short interfering RNA (siRNA) against the *Gas1* transcript. This method lowered GAS1 levels by ~90% with siRNA against *Gas1* but not with control siRNA (Fig. 5B, inset). We then exposed these cells to various concentrations of SHH (conditioned media containing SHH N-terminal product, SHH-N without cholesterol modification) and assayed for HH responsiveness. Between the low concentrations of SHH-N tested, 0.75–12 nM, HH responsiveness is approximately twofold reduced when GAS1 is down-regulated, compared with cells transfected with control siRNA (Fig. 5B). At concentrations >12 nM, the control cell's HH response becomes saturated, while the GAS1 down-regulated cells continue to show progressive increases in HH responsiveness. At 24 nM, the difference in fold induction between the control and GAS1 down-regulated cells becomes statistically insignificant. The physiological
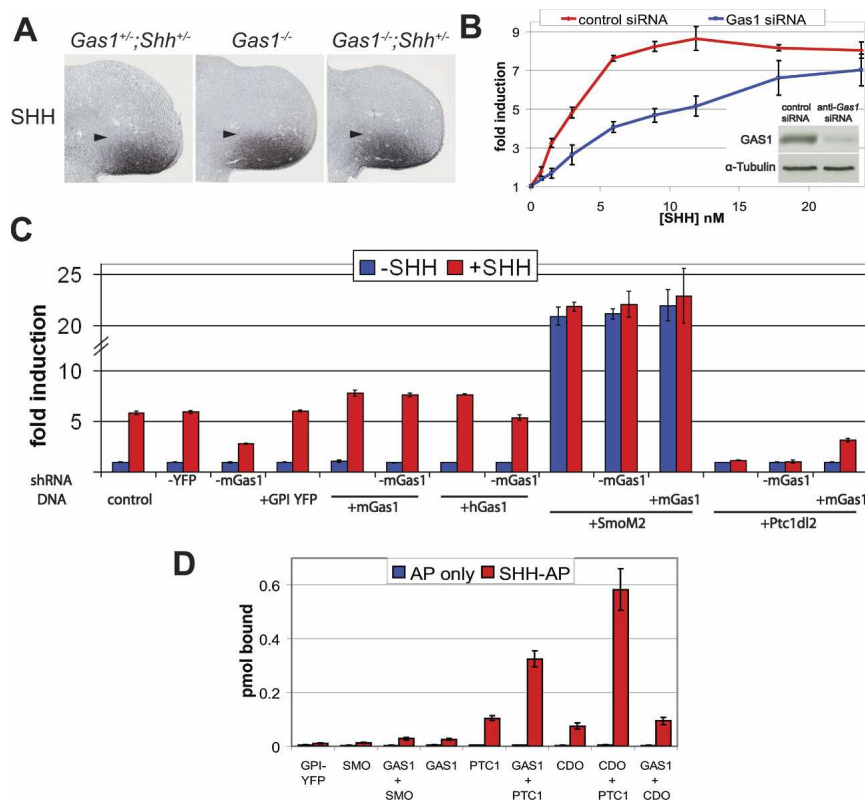
Figure 5. GAS1 facilitates SHH signaling activity. (*A*) SHH IHC on horizontal sections of E10.5 limb buds (*n* = 10) of labeled genotypes; arrowheads mark the anterior boundary of detectable SHH. For color development, *Gas1* mutant limbs were developed for approximately half as long to compensate for the doubled *Shh* dosage. (*B*) Fold induction (*Y*-axis) of NIH3T3-GLI-Luc cells transfected with control siRNA or *Gas1* siRNA by various concentrations of SHH-N (*X*-axis); (*inset*) Western blot for GAS1, then reprobed for α-tubulin as a loading control. (*C*) Fold induction (*Y*-axis) of NIH3T3 cells transiently cotransfected with GLI-Luc reporter and plasmids expressing various effector genes and/or shRNA against *Gas1* (as labeled) in the presence or absence of 10 nM SHH-N. (*D*) SHH-N-AP-binding assay of COS cells expressing *Gas1* and/or *Ptc1*, as well as other control genes are as labeled. They were assayed for binding to SHH-N-AP or AP alone, as determined by the picomoles bound (*Y*-axis) (input = 1.25 nM). In *B–D*, all assays were performed in triplicate; error bars = 1 standard deviation.

relevance of SHH concentrations above the saturation threshold determined for the NIH3T3 cell line is unknown. It is also unclear how much further a reduction in SHH responsiveness would be observed if the siRNA treatment removed all GAS1 protein. Nonetheless, our results suggest that GAS1 indeed enhances HH signaling activity.

To confirm this result with an alternate method, we transiently transfected NIH3T3 cells with the GLI-luciferase reporter and an expression construct for short hairpin RNA (shRNA) against a region in the *Gas1* 3′ untranslated region (UTR) that is a different sequence from that used above. At a concentration of SHH-N just below the threshold of maximal response (10 nM), we find a similar approximately twofold reduction in reporter activity when *Gas1* transcripts were targeted by shRNA compared with the empty shRNA vector control or to shRNA against YFP (Fig. 5C). Conversely, cotransfection with an expression construct for mouse *Gas1* (*mGas1*) causes a modest increase in the HH response, while expression for a GPI-anchored YFP has no effect. Importantly, the decrease in HH responsiveness caused by shRNA against *Gas1* can be rescued by coexpressing a *mGas1* cDNA without the shRNA target sequence. Similarly, an expression construct for human *Gas1* (*hGas1*), which is not a target for the shRNA, could also rescue the HH response, indicating that *hGas1* can function in a similar way as the *mGas1* (Fig. 5C). Thus, we conclude that GAS1 activity is required for maximal HH response in NIH3T3 cells.

Because GAS1 binds to HH at the cell surface (Lee et

al. 2001a), we predict that it acts either at the level of PTC1 or SMO. To test this, we used the above cell culture reporter system to place GAS1 in the HH pathway relative to PTC1 and SMO. As expected, when an activating form of *Smo*, *SmoM2* (Buttitta et al. 2003), was expressed in the NIH3T3 cells, the HH pathway was strongly activated independently of HH (Fig. 5C). Either overexpressing *Gas1* or knocking down *Gas1* did not alter the activity of *SmoM2* in the presence or absence of HH, suggesting that GAS1 acts at or above the level of SMO. Conversely, when a non-HH-binding form of *Ptc1*, *delta-loop2-Ptc1* (*Ptc1dl2*) (Briscoe et al. 2001), was expressed, HH-dependent pathway activation through the endogenous receptor PTC1 was repressed. While reducing GAS1 did not alter the dominant effect of *Ptc1dl2* as expected, expressing more *Gas1* did partially rescue HH responsiveness, indicating that the effect of *Ptc1dl2* can be overcome by *Gas1* overexpression. Taken together, we place GAS1 function above the level of SMO and likely at or below the level of PTC1.

Activation of the HH pathway by HH–PTC1 binding has been proposed to be determined by the ratio between unbound and bound PTC1 (Casali and Struhl 2004). If so, our rescue data predict that increasing GAS1 levels increases the HH-bound PTC1 fraction to overcome the critical ratio required for pathway activation. To investigate this, COS cells transiently expressing either GAS1, PTC1, or simultaneously GAS1 and PTC1 were exposed to conditioned media containing the SHH-N-alkaline phosphatase (SHH-N-AP) fusion protein that allows for quantification of binding (Lee et al. 2001a). As

predicted, cells expressing either GAS1 or PTC1 bind SHH-N-AP at levels 2.3-fold and 9.5-fold, respectively, greater than cells expressing either GPI-anchored YFP or SMO (Fig. 5D). When both GAS1 and PTC1 were expressed, the amount of SHH-N-AP bound was 29.5-fold higher than in the control cells, an amount greater than the sum of binding provided by GAS1 and PTC1 individually. This indicates that the two proteins display synergism in SHH-N-AP binding and suggests that the positive action of GAS1 on HH signaling results from an increase in binding of HH to PTC1. Recently, Ihog was shown to bind Hh and mediate Hh signaling in *Drosophila* (Yao et al. 2006). The mammalian *ihog* homolog is *Cdo*. As a positive control, we confirmed the ability of CDO to bind to SHH-N-AP (6.8-fold) and demonstrated the synergistic binding between CDO and PTC1 (53.0-fold) (Fig. 5D, as predicted in Yao et al. 2006). However, we did not observe a synergistic binding of SHH-N-AP between GAS1 and CDO (8.5-fold, approximately equal to the sum of binding providing by GAS1 and CDO individually). This suggests that GAS1 and CDO function independently of each other to facilitate PTC1 binding to SHH-N.

Increasing *Gas1* expression enhances HH responsiveness in the neural tube

The above results predict that increasing *Gas1* expression should be able to enhance HH signaling in vivo. To test this directly, we turned to the chick neural tube to take advantage of a powerful gene delivery tool; that is, electroporation. In the chicken neural tube, the *Gas1* expression pattern (Lee and Fan 2001) and HH-dependent specification of ventral cell types are similar to those in the mouse (Briscoe and Ericson 1999). We first assessed markers that represent the two ends of the diffusible HH signaling spectrum: PAX7, whose ventral boundary marks the lowest limit of HH signaling readout; and

NKX2.2, which labels the p3 progenitors (located just dorsal to the floorplate) (Briscoe and Ericson 1999). For expression, we constructed an expression plasmid with *mGas1* cDNA followed by an internal ribosomal entry site–green fluorescent protein (IRES-GFP) cassette to monitor *Gas1*-expressing cells. The control plasmid expresses a mutant form of GAS1 with an amino acid 155 glutamine (N) to alanine (A) change (i.e., *Gas1N/A*), which is surface presented but not N-glycosylated and displays minimal SHH binding (Lee et al. 2001a). When the *Gas1N/A* expression plasmid was electroporated into the left side of the chick neural tube, we saw no alteration of PAX7 (Fig. 6A,B) or NKX2.2 (Fig. 6C,D) expression domains compared with the control right side. In contrast, when the *Gas1*-expressing plasmid was used, we observed repression of PAX7 when GFP was present in the dorsal neural tube (Fig. 6E,F). When almost all cells on the electroporated side were GFP-positive, ectopic NKX2.2-positive cells could be found halfway up the neural tube, accompanied by reduced NKX2.2 levels at the normal p3 position (Fig. 6G,H). In neural tubes with segregated GFP-positive cells, we found that the PAX7-repressed domain was always within the GFP-positive domain (Fig. 6I,J), whereas ectopic NKX2.2-positive cells were always GFP-positive (Fig. 6K,L). Similar marker analysis was performed for HNF3β, OLIG2, NKX6.1, and PAX6 in Supplementary Figure S4, and the results are consistent with the conclusions described above. Additionally, we observed that when *Gas1* was overexpressed in only the ventral neural tube, inhibition of HH signaling dorsal to the GFP-positive domain was observed (data not shown), a result probably due to sequestration of HH.

The above results demonstrate the following points: First, ectopic GAS1 can enhance HH signaling and alter the response gradient in the neural tube; second, this activity of GAS1 depends on its HH-binding property; and third, GAS1 appears to enhance HH signaling in a cell-autonomous manner. Together with the data that
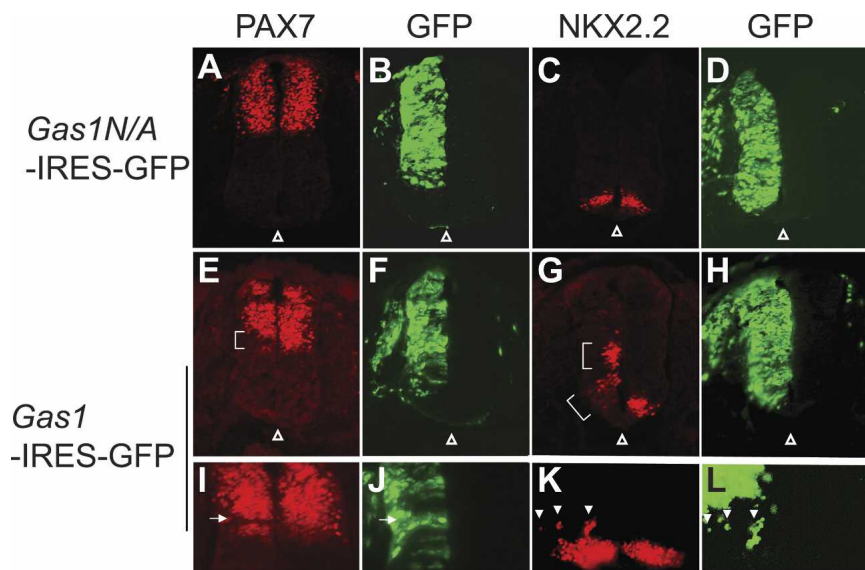
Figure 6. *Gas1* expression alters the position of neuronal progenitors in the neural tube. Chick trunk neural tube was electroporated with *Gas1N/A*-IRES-GFP (*A–D*) or *Gas1*-IRES-GFP (*E–L*) plasmids and analyzed for GFP (*B,D,F,H,J,L*), PAX7 (*A,E,I*), and NKX2.2 (*C,G,K*) by double immunofluorescence (green for GFP, and red for PAX7 or NXK2.2) on the same sections. Each pair of images (*A* and *B*, *C* and *D*, etc.) is from the same section; $n \geq 10$ for each pair. *I–L* are at 2× higher magnification than *A–H*. Brackets indicate altered domains of PAX7 or NKX2.2, arrows indicate corresponding PAX7-negative and GFP-positive domains, arrowheads denote NKX2.2 and GFP doubly positive cells, and open arrowheads indicate the ventral midline.

GAS1 and PTC1 display synergistic binding to SHH, our data strongly support the possibility that GAS1 facilitates HH binding to PTC1 to enhance HH responsiveness in receiving cells.

Shh *regulates* Gas1 *expression*

The above data indicate that *Gas1* acts as a positive regulator of HH signaling. Somewhat counterintuitively, *Gas1* expression levels negatively correlate with HH signaling levels; that is, *Ptc1* expression. This expression pattern implies that *Gas1* is repressed by high-level HH signaling, which may represent a HH self-imposed regulatory loop to modulate its own signaling activity. To test this, we used the *LacZ* gene knocked into the *Gas1* locus to report for *Gas1* expression by X-gal staining. In the E9.5 *Gas1*^+/−;*Shh*^+/− embryo at the trunk level, X-gal staining was present in the dorsal neural tube and somites (Fig. 7A). We noted that the staining was throughout the neural plate at the tail region, and became progressively dorsally restricted in more anterior sections (Supplementary Fig. S5), suggesting that increasing HH levels gradually repress *Gas1* expression. Consistent with this, X-gal staining was found in the
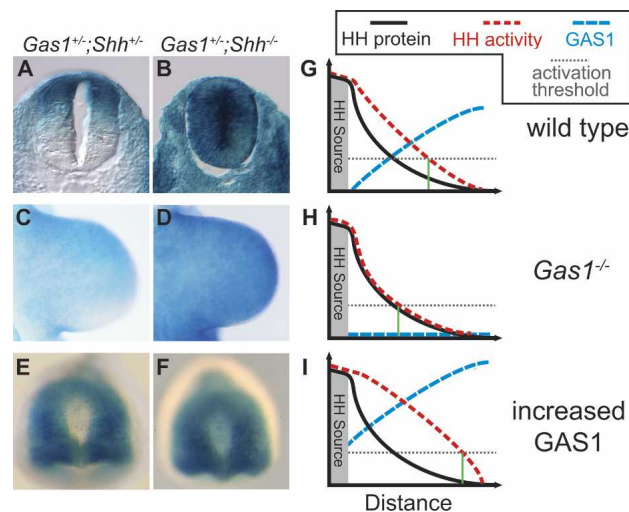
entire neural tube and somites of *Gas1*^+/−;*Shh*^−/− embryos at all levels (Fig. 7B; data not shown). The presence of *Gas1* in the early neural plate prior to its down-regulation likely helps SHH secreted from the notochord to induce the floorplate, explaining the partial floorplate defect in the *Gas1* mutant (Fig. 2V; Supplementary Fig. S2).

In the E10.5 *Gas1*^+/−;*Shh*^+/− forelimb buds, X-gal staining was present in a gradient counter to that of high levels of HH signaling, but the staining in the *Gas1*^+/−;*Shh*^−/− embryo was throughout the entire limb bud (Fig. 7C,D). Thus, *Gas1* and *Ptc1* are oppositely regulated by HH signaling: *Gas1* is down-regulated and *Ptc1* is up-regulated. Despite this, the *Gas1* and *Ptc1* expression domains overlap in the middle regions of the limb bud (Lee et al. 2001a; data not shown), a location where low-level HH is known to act. We propose that at the regions where it is expressed, GAS1 exerts its activity to facilitate HH-PTC1 binding and enhance HH activity. The enhancement of specifically low-level HH signaling distant from the HH source in the limb bud is presumably due to a lack of *Gas1* expression in the posterior mesenchyme even prior to ZPA formation, consistent with a lack of phenotype in the *Gas1*^−/− posterior limb. How *Gas1* expression is restricted from the posterior limb bud prior to *Shh* expression is currently unknown.

The above results led us to re-examine whether *Gas1* expression, regulation, and function for left/right heart asymmetry follow the same logic as for the neural tube, somite, and limb. Indeed, in E8.0 embryos, *Gas1* expression inferred from X-gal staining was found in cells surrounding and posterior to the node, where HH signaling is crucial for specifying left–right asymmetry (Fig. 7E; Zhang et al. 2001). In the *Gas1*^+/−;*Shh*^−/− embryo, X-gal-positive cells were found within the node (Fig. 7F), consistent with *Gas1* expression being negatively regulated by HH signaling. *Gas1*^−/−;*Shh*^−/− embryos had a further intensified X-gal signal accompanied by a lack of detectable *Ptc1* expression in the node, supporting that the left–right asymmetry defect noted in the *Shh*^−/−;*Gas1*^−/− embryo is due to a further reduction in HH signaling compared with the *Shh*^−/− embryo (Supplementary Fig. S6). Based on the regulation of *Gas1*, we propose that it is a negative feedback mechanism to restrain HH signaling activity.

Figure 7. HH signaling negatively regulates *Gas1* expression. *Gas1* expression was determined by X-gal staining in E9.5 neural tubes at forelimb level (*A,B*), E10.5 limb buds viewed dorsally (*C,D*), and E8.0 nodes viewed ventrally (*E,F*). Genotypes are labeled on *top* of each panel. (*G–I*) Model for the role of *Gas1* in transforming a hypothetical HH concentration gradient to an activity gradient. The *Y*-axis represents the magnitudes of three gradients: HH concentration (black line), HH activity (red dashed line), and GAS1 levels (blue dashed line). The *X*-axis represents a HH source and the distance from that source. The shape of the HH protein gradient is based in part on mathematical modeling (Saha and Schaffer 2006). GAS1 levels have direct implications for HH activity gradients and the distance from the HH source (green line) where the activation threshold (dashed gray line) for a hypothetical target gene is reached. For simplification, the contributions of other known HH-modifying proteins are not included in this model.

Discussion

We show here that *Gas1* is a positive regulator of HH signaling in all five developmental contexts examined. Retrospectively, the microphthalmia (Lee et al. 2001b) and reduced cerebellum size (Liu et al. 2001) of the *Gas1* mutant are likely also due to reduced HH signaling as *Shh* plays important roles in both contexts. The pleiotropic involvement of *Gas1* in HH-directed embryonic patterning implies that it is an integral component of the HH pathway. To extend our findings, we propose that *Gas1* may well be a modifier locus for the holoprosencephaly caused by reduced HH signaling and also possi-

bly an enhancer of tumorigenesis associated with increased HH signaling.

GAS1's HH-binding property and its ability to enhance HH activity are reminiscent of the recently described CDO and BOC proteins (Tenzen et al. 2006; Zhang et al. 2006), which are homologs of Ihog and Boi, respectively, in *Drosophila* (Yao et al. 2006). Like Ihog (Yao et al. 2006) and CDO (this study), GAS1 can also synergize with PTC1 to bind HH. Although their expression and regulation are similar, there are differences between *Gas1* and *Cdo/Boc.* For example, *Cdo* is expressed in the E9.5 notochord and floorplate, indicating that it is not regulated in the exact same manner as *Gas1*. Additionally, the *Cdo* mutant phenotype appears limited to defects in midline structures (Zhang et al. 2006) and a delay in myogenesis (Cole et al. 2004), while the *Boc* mutant phenotype appears limited to axon guidance (Connor et al. 2005; Okada et al. 2006). Perhaps the lack of complete loss of HH signaling in each single mutant is because these genes are able to partially compensate for each other in places where they are coexpressed. This possibility has been examined between *Gas1* and *Cdo* in the accompanying study (Allen et al. 2007).

It is also possible that there is a specific context-dependent requirement for each of the genes to mediate HH signaling. The differential requirement for *Gas1* versus *Cdo/Boc* in different contexts may not be surprising because CDO/iHog and BOC/Boi are highly related Fibronectin type III repeat-containing proteins, while GAS1 belongs to the Glial Cell-Derived Neurotrophic Factor Receptor α (GDNFRα or GFRα) family (Cabrera et al. 2006). Sequence alignments between GFRα-domain-containing genes of various species predicted that *Caenorhabditis elegans* and honey bee genomes might have a *Gas1* homolog (Schueler-Furman et al. 2006). However, the single N-glycosylation site in GAS1 required for HH binding is conserved among vertebrate GAS1 proteins but not found in the presumed invertebrate GAS1 proteins, suggesting that invertebrate GAS1 homologs do not function in the HH pathway. Perhaps through convergent evolution, *Gas1* has acquired the ability to bind HH and enhance its signaling similarly to the conserved *Cdo/Boc* family and may be a novel addition to the HH signaling core pathway in vertebrates. Interestingly, GAS1 still retains the ability to modulate GDNF signaling. Given that SHH is involved in adult neurogenesis (Ahn and Joyner 2005) and that GDNF is a potent neuroprotective factor (Schueler-Furman et al. 2006), *Gas1* may have evolved to be a nodal point for the convergence of these two important signaling pathways in the adult brain.

The observed negative regulation of *Gas1* by HH signaling is in stark contrast to the positive regulation of PTC1 by HH signaling. PTC1 up-regulation has been proposed to attenuate HH diffusion and provides self-imposed regulation on its distance of action. Conversely, our data support a model in which HH down-regulates GAS1 to restrain its own activity. As HH concentration increases, *Gas1* is correspondingly down-regulated to a level appropriate for the required magnitude of signaling

amplification. This does not preclude that GAS1 can enhance local signaling. For example, the presence of GAS1 in the early neural plate prior to its down-regulation appears to be required for complete floorplate induction by SHH from the notochord. A caveat to this model is that in the posterior limb, where due to an unknown mechanism, *Gas1* is not expressed prior to *Shh* expression in the ZPA and therefore cannot facilitate local signaling (Liu et al. 2002). Previous studies using explants of presomitic mesoderm (Lee et al. 2001a) and mandibular mesenchyme (Cobourne et al. 2004) found that overexpressed GAS1 inhibited SHH signaling. It is possible that explants cultured in vitro lost the capacity to regulate/provide additional components necessary for GAS1 to act positively. However, a more likely explanation is that the inhibitory effects seen were due to sequestration of SHH by excessive GAS1, since under certain conditions we also observed a non-cell-autonomous inhibitory effect of GAS1 in our electroporation assay (Allen et al. 2007; data not shown). It appears that how the HH response is modulated by GAS1 is dependent on the levels of GAS1 and HH, and possibly the cell type. Whether in vivo contexts exist where high levels of GAS1 can inhibit HH signaling is an intriguing possibility.

In our model, upon GAS1 gradient formation, the HH concentration gradient is steeper than its activity gradient, owing to the enhancement by GAS1 (Fig. 7G). When *Gas1* is removed, the HH activity gradient becomes close to the HH protein gradient (Fig. 7H). Conversely, when *Gas1* levels are increased, the contour of the HH activity gradient becomes inflated (Fig. 7I). In both altered situations, shifts in the positions of the cell types being specified will occur. Thus, simultaneous up-regulation of a repressor (PTC1) and down-regulation of an enhancer of HH activity (GAS1) may not be essential for creating a signaling gradient per se, but can be instrumental to further refine multiple thresholds within the target field governed by HH, likely part of an evolutionary process for building the increasing intricacy of vertebrate form and function.

Materials and methods

Generation of mutant Gas1 mice

See Supplementary Figure 1.

Generation of embryos

Mutant alleles of *Shh* (Chiang et al. 1996) and *Gas1* were maintained on a mixed 129/Sv; C57BL6/J background. Noon of the vaginal plug date was considered E0.5. Genotypes were determined by PCR with yolk sac DNA using the following primers: for the *Gas1* wild-type allele, 5′-TACTGCGGCAAGCTTTT CAACGG-3′ and 5′-AGCGCGCTGCTCGTCGTCATATTC-3′; for the *Gas1* mutant allele, 5′-ACTACGCGTACTGTGA GCCAGAG-3′ and 5′-AGTGACCAGCGAATACCTGTTCC-3′; for the *Shh* wild-type allele, 5′-GACCATGTCTGCACACT TAGGTTCC-3′ and 5′-GAAGGCCAGGAGGAGAAGGCTC AC-3′; for the *Shh* mutant allele, 5′-CGTGCAGTTCACTCA CAAGGCACT-3′ and 5′-ACGAGTTCTTCTGAGGGGATC-3′.

Histology/LacZ stains

For histology, embryos were fixed in methacarn, embedded in paraffin, sectioned at 6 µm, and stained by hematoxylin and eosin (Surgipath). For LacZ stains, embryos were fixed in glutaraldehyde and stained in X-gal or S-gal as described (Hogan et al. 1994).

ISH

ISH on paraffin sections (10 µm) using digoxigenin-UTP (DIG)-labeled antisense probes was performed for *Pax1*, *Pax3* (Fan and Tessier-Lavigne 1994), *Ptc1* (gift from M. Scott, Stanford University, Stanford, CA), and *Dbx1*. The template for *Dbx1* probe synthesis was a PCR-amplified 2-kb mouse *Dbx1* cDNA using the primer sequences 5′-GGTTACCAGGATACTGAGCCAAA GAG-3′ and 5′-AAAATAATGAGA GGGACACAGCCAGC-3′, cloned into pCR-TOPOII (Invitrogen), and transcribed by T7. Images were photographed using DIC microscopy. Whole-mount ISH using DIG-labeled antisense probes was performed following standard procedures (Wilkinson 1992) for *Fgf4*, *Gli1* (gifts from C.C. Hui, Sick Kids, University of Toronto, Toronto, Ontario, Canada), *Grem* (gift from R. Zeller, Utrecht University, Utrecht, The Netherlands), *Shh* (gift from A. McMahon, Harvard University, Cambridge, MA), and *Ptc1*. Images were photographed using a dissecting microscope.

IHC

SHH and IHH IHC was performed using Sainte Marie's fixative (Gritli-Linde et al. 2001). The primary antibody (Ab80) was provided by A. McMahon and used at a 1:500 dilution, followed by biotinylated goat anti-rabbit (Vector Laboratories) antibody (1:500). For other IHC, embryos were cryosectioned (10 µm) following a 45-min fixation in 4% paraformaldehyde/phosphate buffer (pH 7.2) at 4°C. PAX6, PAX7, NKX6.1, NKX2.2, and HNF3β mouse monoclonal antibodies (DSHB) were used at a 1:10 dilution. Antibodies against DBX1 and GSH1/2 were gifts from T. Jessell (Columbia University, New York, NY) and M. Goulding (Salk Institute, La Jolla, CA), respectively. Rabbit anti-OLIG2 was purchased from Chemicon. Appropriate HRP-conjugated secondary antibodies (Vector Laboratories) were used at 1:500. For visualization, DAB color development was used. Images were photographed using DIC microscopy.

Skeleton preparation

Harvested limbs were incubated in water overnight. Skin was removed following a 10-min incubation at 65°C, then limbs were fixed in ethanol for 5 d and acetone for 2 d, and stained for 3 d in 67% ethanol/5% glacial acetic acid/23% H_2O with 0.005% (w/v) Alizarin Red S (Sigma) and 0.005% (w/v) Alcian Blue 8GX (Sigma). Tissue was cleared with 1% (w/v) KOH, then serially switched to increasing amounts of glycerol. Photographs were taken in 100% glycerol using a dissecting microscope.

Western blots

E10.5 limb buds were harvested and dissected into halves then lysed in 15 µL of ice cold RIPA buffer plus protease inhibitors. Nuclei were removed by centrifugation, and lysates were resolved by 5% SDS-PAGE. Immunoblotting was performed using rabbit GLI-3 H-280 (Santa Cruz Biotechnology) followed by HRP-conjugated secondary antibody and ECL detection (Amer-

sham). Band intensities were quantified with ImageQuant TL (Amersham Biosciences).

Cell culture, conditioned media (CM), and transfection assays

COS, 293T (ATCC), NIH3T3, and NIH3T3-GLI-Luc cells (gift from P. Beachy, Stanford University, Stanford, CA) were cultured in DMEM (high glucose) with 10% fetal bovine serum, penicillin, and streptomycin (Invitrogen). Control and SHH-N CM were produced by 293T cells transfected with 12 µg of pRK5 and 12 µg of pRK5-SHH-N (Fan et al. 1995), respectively, plus 30 µL of Fugen6 HD (Roche) in a 10-cm dish. CM was collected for five consecutive days. The activities of SHH-N were determined by applying CM to NIH3T3-GLI-Luc cells for 48 h and assaying for luciferase activity (Promega) using D-luciferin (Sigma). Fold induction was calculated as luciferin light-emitting units from extracts of cells exposed to SHH-N CM/control CM after normalization to total protein. SHH-N concentrations were determined by side-by-side comparison using Western blotting and measuring the band intensity of SHH-N in the CM relative to serially diluted known amounts of bacterially produced SHH-N (BCA assay; Pierce).

For siRNA transfection assays, we used modified synthetic siRNA from Invitrogen (Stealth RNAi). Cells were transfected in 12-well dishes at ~80% confluence with 14.7 µL of 20 µM siRNA and 3 µL of Lipofectamine 2000 (Invitrogen). For control, Stealth RNAi Negative Control Medium GC was used. For siRNA against *Gas1*, equal amounts of the following sequences were used: 5′-GCUGCAGAGAUAACCGGCUGAUCUA-3′ and 5′-CGGCUGAUCUAUACUGCCAGCUCUA-3′. Two days after transfection, SHH-N CM was applied, and cells were harvested for luciferase assays 2 d later.

For shRNA assays, parental NIH3T3 cells were used. The pRNATin-H2.1/Hygro (GenScript) vector was used for expression. Of three short hairpins tested, two were effective in knocking down mGAS1 in stable lines (by hygromycin selection). Their double-stranded regions correspond to nucleotides 936–954 (in the coding region) and nucleotides 1990–2010 (in the 3′ UTR) of *mGas1* (NM 008,086). The results shown here are from the latter (named O3). The sequence of shRNA against YFP was as described (Yao et al. 2006). Cells in a 12-well dish were transfected using 7 µL of Perfectin (Gelantis) with 1 µg of pRNATin-H2.1/Hygro or pRNATin-H2.1/Hygro-O3, together with 0.25 µg of a GLI-Luc reporter (Buttitta et al. 2003), 0.25 µg of pSV-bgal (GIBCO), and 1 µg of an effector plasmid per well. The effector plasmids are pTK (modified from pRL-TK; Promega), pTK-GPI-YFP, pTK-*mGas1*, pTK-*hGas1*, pcDNA3-*SmoM2*, and pTK-*Ptc1dl2*. *Ptc1dl2* was a gift from G. Struhl (Columbia University, New York, NY), and *SmoM2* was from Genentech. Thirty-six hours after transfection, SHH-N or control CM was applied; 36 h later, cells were harvested for luciferase and β-gal (using o-nitrophenyl β-D-galactopyranoside [Sigma], followed by OD_{420nm}) assays. Fold induction was calculated as described above after normalization to β-gal activity.

For the surface binding assay, COS cells in six-well dishes were transfected with 2 µg of expression vectors with 5 µL of Fugen6 HD per well. pcDNA3-GPI-YFP, pcDNA3-*Gas1*, pcDNA3-*Ptc1*, pcDNA3-*Smo*, and pcDNA-*Cdo* were used. The *Ptc1* cDNA was a gift from M. Scott. GPI-YFP was a gift from M. Edidin (Johns Hopkins University, Baltimore, MD). The *Cdo* cDNA was from an I.M.A.G.E. clone. Forty-eight hours after transfection, SHH-N-AP and control AP CM were applied. SHH-N-AP and AP CM, and ligand binding and bound AP activity measuring (using p-nitrophenyl phosphate [Sigma], fol-

lowed by OD_{405nm}) conditions were as described (Lee et al. 2001a).

Chick neural tube electroporation

mGas1 and *mGas1N/A* (Lee et al. 2001a) were cloned into a pCIG-IRES-GFP vector (gift from A. McMahon) to construct pCIG-*mGas1*-IRES-GFP and pCIG-*mGas1N/A*-IRES-GFP. Hamilton and Hamberger (HH) stage 11–12 chick embryos (SPAFAS) were injected with expression plasmids at 0.75 µg/µL into the neural tube, followed by five pulses of 30 V at 50 msec per pulse with 950-msec intervals, and then incubated to stage 20–22. Embryos with visible GFP autofluorescence in the spinal cord (trunk level) were processed for immunofluorescence using the primary antibodies described above, and to GFP (Torre Pines; rabbit polyclonal, 1:1000), and followed by goat anti-mouse (rhodamine-conjugated, 1:500) and goat anti-rabbit (fluorescein-conjugated, 1:500) secondary antibodies. Slides were mounted in Flouromount G (Southern Biotechnology) and photographed using fluorescent microscopy.

References

Ahn, S. and Joyner, A.L. 2004. Dynamic changes in the response of cells to positive hedgehog signaling during mouse limb patterning. *Cell* **118:** 505–516.

Ahn, S. and Joyner, A.L. 2005. In vivo analysis of quiescent adult neural stem cells responding to Sonic hedgehog. *Nature* **437:** 894–897.

Allen, B.L., Tenzen, T., and McMahon, A.P. 2007. The Hedgehog-binding proteins Gas1 and Cdo cooperate to positively regulate Shh signaling during mouse development. *Genes & Dev.* (this issue) doi: 10.1101/gad.1543607.

Briscoe, J. and Ericson, J. 1999. The specification of neuronal identity by graded Sonic Hedgehog signalling. *Semin. Cell Dev. Biol.* **10:** 353–362.

Briscoe, J., Sussel, L., Serup, P., Hartigan-O'Connor, D., Jessell, T.M., Rubenstein, J.L., and Ericson, J. 1999. Homeobox gene Nkx2.2 and specification of neuronal identity by graded Sonic hedgehog signalling. *Nature* **398:** 622–627.

Briscoe, J., Chen, Y., Jessell, T.M., and Struhl, G. 2001. A hedgehog-insensitive form of patched provides evidence for direct long-range morphogen activity of sonic hedgehog in the neural tube. *Mol. Cell* **7:** 1279–1291.

Buttitta, L., Mo, R., Hui, C.C., and Fan, C.M. 2003. Interplays of Gli2 and Gli3 and their requirement in mediating Shh-dependent sclerotome induction. *Development* **130:** 6233–6243.

Cabrera, J.R., Sanchez-Pulido, L., Rojas, A.M., Valencia, A., Manes, S., Naranjo, J.R., and Mellstrom, B. 2006. Gas1 is related to the glial cell-derived neurotrophic factor family receptors α and regulates Ret signaling. *J. Biol. Chem.* **281:** 14330–14339.

Casali, A. and Struhl, G. 2004. Reading the Hedgehog morphogen gradient by measuring the ratio of bound to unbound Patched protein. *Nature* **431:** 76–80.

Chen, Y. and Struhl, G. 1996. Dual roles for Patched in sequestering and transducing Hedgehog. *Cell* **87:** 553–563.

Chiang, C., Litingtung, Y., Lee, E., Young, K.E., Corden, J.L., Westphal, H., and Beachy, P.A. 1996. Cyclopia and defective axial patterning in mice lacking Sonic hedgehog gene function. *Nature* **383:** 407–413.

Chiang, C., Litingtung, Y., Harris, M.P., Simandl, B.K., Li, Y., Beachy, P.A., and Fallon, J.F. 2001. Manifestation of the limb prepattern: Limb development in the absence of Sonic hedgehog function. *Dev. Biol.* **236:** 421–435.

Cobourne, M.T., Miletich, I., and Sharpe, P.T. 2004. Restriction of Sonic hedgehog signalling during early tooth development. *Development* **131:** 2875–2885.

Cole, F., Zhang, W., Geyra, A., Kang, J.S., and Krauss, R.S. 2004. Positive regulation of myogenic bHLH factors and skeletal muscle development by the cell surface receptor CDO. *Dev. Cell* **7:** 843–854.

Connor, R.M., Allen, C.L., Devine, C.A., Claxton, C., and Key, B. 2005. BOC, brother of CDO, is a dorsoventral axon-guidance molecule in the embryonic vertebrate brain. *J. Comp. Neurol.* **485:** 32–42.

Del Sal, G., Collavin, L., Ruaro, M.E., Edomi, P., Saccone, S., Valle, G.D., and Schneider, C. 1994. Structure, function, and chromosome mapping of the growth-suppressing human homologue of the murine gas1 gene. *Proc. Natl. Acad. Sci.* **91:** 1848–1852.

Ericson, J., Muhr, J., Jessell, T.M., and Edlund, T. 1995a. Sonic hedgehog: A common signal for ventral patterning along the rostrocaudal axis of the neural tube. *Int. J. Dev. Biol.* **39:** 809–816.

Ericson, J., Muhr, J., Placzek, M., Lints, T., Jessell, T.M., and Edlund, T. 1995b. Sonic hedgehog induces the differentiation of ventral forebrain neurons: A common signal for ventral patterning within the neural tube. *Cell* **81:** 747–756.

Ericson, J., Morton, S., Kawakami, A., Roelink, H., and Jessell, T.M. 1996. Two critical periods of Sonic Hedgehog signaling required for the specification of motor neuron identity. *Cell* **87:** 661–673.

Evdokiou, A. and Cowled, P.A. 1998. Growth-regulatory activity of the growth arrest-specific gene, GAS1, in NIH3T3 fibroblasts. *Exp. Cell Res.* **240:** 359–367.

Fan, C.M. and Tessier-Lavigne, M. 1994. Patterning of mammalian somites by surface ectoderm and notochord: Evidence for sclerotome induction by a hedgehog homolog. *Cell* **79:** 1175–1186.

Fan, C.M., Porter, J.A., Chiang, C., Chang, D.T., Beachy, P.A., and Tessier-Lavigne, M. 1995. Long-range sclerotome induction by Sonic hedgehog: Direct role of the amino-terminal cleavage product and modulation by the cyclic AMP signaling pathway. *Cell* **81:** 457–465.

Goodrich, L.V., Johnson, R.L., Milenkovic, L., McMahon, J.A., and Scott, M.P. 1996. Conservation of the hedgehog/patched signaling pathway from flies to mice: Induction of a mouse patched gene by Hedgehog. *Genes & Dev.* **10:** 301–312.

Gritli-Linde, A., Lewis, P., McMahon, A.P., and Linde, A. 2001. The whereabouts of a morphogen: Direct evidence for short- and graded long-range activity of hedgehog signaling peptides. *Dev. Biol.* **236:** 364–386.

Harfe, B.D., Scherz, P.J., Nissim, S., Tian, H., McMahon, A.P., and Tabin, C.J. 2004. Evidence for an expansion-based temporal Shh gradient in specifying vertebrate digit identities. *Cell* **118:** 517–528.

Hogan, B., Beddington, R., Costantini, F., and Lacey, E. 1994. *Manipulating the mouse embryo*, 2nd ed. Cold Spring Harbor Laboratory Press, Cold Spring Harbor, NY.

Kayed, H., Kleeff, J., Osman, T., Keleg, S., Buchler, M.W., and

Friess, H. 2006. Hedgehog signaling in the normal and diseased pancreas. *Pancreas* **32:** 119–129.

Kraus, P., Fraidenraich, D., and Loomis, C.A. 2001. Some distal limb structures develop in mice lacking Sonic hedgehog signaling. *Mech. Dev.* **100:** 45–58.

Lee, C.S. and Fan, C.M. 2001. Embryonic expression patterns of the mouse and chick Gas1 genes. *Mech. Dev.* **101:** 293–297.

Lee, C.S., Buttitta, L., and Fan, C.M. 2001a. Evidence that the WNT-inducible growth arrest-specific gene 1 encodes an antagonist of sonic hedgehog signaling in the somite. *Proc. Natl. Acad. Sci.* **98:** 11347–11352.

Lee, C.S., May, N.R., and Fan, C.M. 2001b. Transdifferentiation of the ventral retinal pigmented epithelium to neural retina in the growth arrest specific gene 1 mutant. *Dev. Biol.* **236:** 17–29.

Lewis, P.M., Dunn, M.P., McMahon, J.A., Logan, M., Martin, J.F., St-Jacques, B., and McMahon, A.P. 2001. Cholesterol modification of sonic hedgehog is required for long-range signaling activity and effective modulation of signaling by Ptc1. *Cell* **105:** 599–612.

Litingtung, Y. and Chiang, C. 2000a. Control of Shh activity and signaling in the neural tube. *Dev. Dyn.* **219:** 143–154.

Litingtung, Y. and Chiang, C. 2000b. Specification of ventral neuron types is mediated by an antagonistic interaction between Shh and Gli3. *Nat. Neurosci.* **3:** 979–985.

Litingtung, Y., Dahn, R.D., Li, Y., Fallon, J.F., and Chiang, C. 2002. Shh and Gli3 are dispensable for limb skeleton formation but regulate digit number and identity. *Nature* **418:** 979–983.

Liu, Y., May, N.R., and Fan, C.M. 2001. Growth arrest specific gene 1 is a positive growth regulator for the cerebellum. *Dev. Biol.* **236:** 30–45.

Liu, Y., Liu, C., Yamada, Y., and Fan, C.M. 2002. Growth arrest specific gene 1 acts as a region-specific mediator of the Fgf10/Fgf8 regulatory loop in the limb. *Development* **129:** 5289–5300.

Marigo, V. and Tabin, C.J. 1996. Regulation of patched by sonic hedgehog in the developing neural tube. *Proc. Natl. Acad. Sci.* **93:** 9346–9351.

McMahon, A.P., Ingham, P.W., and Tabin, C.J. 2003. Developmental roles and clinical significance of hedgehog signaling. *Curr. Top. Dev. Biol.* **53:** 1–114.

Okada, A., Charron, F., Morin, S., Shin, D.S., Wong, K., Fabre, P.J., Tessier-Lavigne, M., and McConnell, S.K. 2006. Boc is a receptor for sonic hedgehog in the guidance of commissural axons. *Nature* **444:** 369–373.

Pepinsky, R.B., Zeng, C., Wen, D., Rayhorn, P., Baker, D.P., Williams, K.P., Bixler, S.A., Ambrose, C.M., Garber, E.A., Miatkowski, K., et al. 1998. Identification of a palmitic acid-modified form of human Sonic hedgehog. *J. Biol. Chem.* **273:** 14037–14045.

Pierani, A., Moran-Rivard, L., Sunshine, M.J., Littman, D.R., Goulding, M., and Jessell, T.M. 2001. Control of interneuron fate in the developing spinal cord by the progenitor homeodomain protein Dbx1. *Neuron* **29:** 367–384.

Porter, J.A., Young, K.E., and Beachy, P.A. 1996. Cholesterol modification of hedgehog signaling proteins in animal development. *Science* **274:** 255–259.

Roessler, E. and Muenke, M. 2003. How a Hedgehog might see holoprosencephaly. *Hum. Mol. Genet.* **12:** R15–R25.

Saha, K. and Schaffer, D.V. 2006. Signal dynamics in Sonic hedgehog tissue patterning. *Development* **133:** 889–900.

Schneider, C., King, R.M., and Philipson, L. 1988. Genes specifically expressed at growth arrest of mammalian cells. *Cell* **54:** 787–793.

Schueler-Furman, O., Glick, E., Segovia, J., and Linial, M. 2006. Is GAS1 a co-receptor for the GDNF family of ligands? *Trends Pharmacol. Sci.* **27:** 72–77.

Tanabe, Y., Roelink, H., and Jessell, T.M. 1995. Induction of motor neurons by Sonic hedgehog is independent of floor plate differentiation. *Curr. Biol.* **5:** 651–658.

Tenzen, T., Allen, B.L., Cole, F., Kang, J.S., Krauss, R.S., and McMahon, A.P. 2006. The cell surface membrane proteins Cdo and Boc are components and targets of the Hedgehog signaling pathway and feedback network in mice. *Dev. Cell* **10:** 647–656.

Wang, B., Fallon, J.F., and Beachy, P.A. 2000. Hedgehog-regulated processing of Gli3 produces an anterior/posterior repressor gradient in the developing vertebrate limb. *Cell* **100:** 423–434.

Wijgerde, M., McMahon, J.A., Rule, M., and McMahon, A.P. 2002. A direct requirement for Hedgehog signaling for normal specification of all ventral progenitor domains in the presumptive mammalian spinal cord. *Genes & Dev.* **16:** 2849–2864.

Wilkinson, D.G. 1992. *In situ hybridization: A practical approach.* Oxford University Press, Oxford.

Xie, J. 2005. Hedgehog signaling in prostate cancer. *Future Oncol.* **1:** 331–338.

Yao, S., Lum, L., and Beachy, P. 2006. The ihog cell-surface proteins bind Hedgehog and mediate pathway activation. *Cell* **125:** 343–357.

Zeng, X., Goetz, J.A., Suber, L.M., Scott Jr., W.J., Schreiner, C.M., and Robbins, D.J. 2001. A freely diffusible form of Sonic hedgehog mediates long-range signalling. *Nature* **411:** 716–720.

Zhang, X.M., Ramalho-Santos, M., and McMahon, A.P. 2001. Smoothened mutants reveal redundant roles for Shh and Ihh signaling including regulation of L/R asymmetry by the mouse node. *Cell* **105:** 781–792.

Zhang, W., Kang, J.S., Cole, F., Yi, M.J., and Krauss, R.S. 2006. Cdo functions at multiple points in the Sonic Hedgehog pathway, and Cdo-deficient mice accurately model human holoprosencephaly. *Dev. Cell* **10:** 657–665.